JACS Au
AN OPEN ACCESS JOURNAL OF THE AMERICAN CHEMICAL SOCIETY

pubs.acs.org/jacsau

Article

Porphyrin-Based Multicomponent Metallacage: Host–Guest Complexation toward Photooxidation-Triggered Reversible Encapsulation and Release

Zeyuan Zhang, Lingzhi Ma, Fang Fang, Yali Hou, Chenjie Lu, Chaoqun Mu, Yafei Zhang, Haifei Liu, Ke Gao, Ming Wang, Zixi Zhang, Xiaopeng Li, and Mingming Zhang*

Cite This: *JACS Au* 2022, 2, 1479–1487

Read Online

ACCESS | Metrics & More | Article Recommendations | Supporting Information

ABSTRACT: The development of supramolecular hosts with effective host–guest properties is crucial for their applications. Herein, we report the preparation of a porphyrin-based metallacage, which serves as a host for a series of polycyclic aromatic hydrocarbons (PAHs). The association constant between the metallacage and coronene reaches 2.37 × 10^7 M^{-1} in acetonitrile/chloroform (ν/ν = 9/1), which is among the highest values in metallacage-based host–guest complexes. Moreover, the metallacage exhibits good singlet oxygen generation capacity, which can be further used to oxidize encapsulated anthracene derivatives into anthracene endoperoxides, leading to the release of guests. By employing 10-phenyl-9-(2-phenylethynyl)anthracene whose endoperoxide can be converted back by heating as the guest, a reversible controlled release system is constructed. This study not only gives a type of porphyrin-based metallacage that shows desired host–guest interactions with PAHs but also offers a photooxidation-responsive host–guest recognition motif, which will guide future design and applications of metallacages for stimuli-responsive materials.

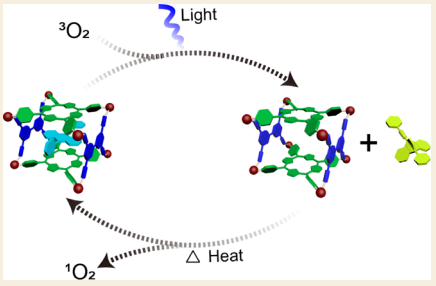

KEYWORDS: *multicomponent metallacages, porphyrin, host–guest complexation, photooxidation, reversible encapsulation and release*

INTRODUCTION

The design and preparation of supramolecular hosts, which can effectively encapsulate guest molecules remain a central theme of supramolecular chemistry.[1,2] Such host–guest systems possess good selectivity, high efficiency, and stimuli responsiveness, enabling their wide applications in the construction of advanced supramolecular materials.[3,4] So far, numerous host systems have been developed including, but not limited to, crown ethers,[5−7] cyclodextrins,[8,9] calixarenes,[10,11] cucurbiturils,[12,13] cyclophanes,[14,15] and pillararenes[16,17] for a wide array of applications in sensing,[18,19] separation and purification,[20,21] transportation,[22,23] drug delivery and release,[24,25] etc. These covalent hosts possess enhanced stabilities, which enable them to be ideal building blocks for the preparation of robust materials. Their functionalization, however, is generally tedious and time-consuming and sometimes quite challenging, especially for water-soluble hosts such as cucurbiturils.[26,27] Directional self-assembly is emerging as an alternative approach for providing noncovalently linked supramolecular hosts with tunable and adjustable cavities.[28,29] Moreover, further functionalities can be readily introduced into the noncovalent hosts via the selection and modification of building blocks toward advanced applications.[30,31]

Owing to their moderate bond strength and well-defined directionality, metal-coordination interactions have proved to be ideal noncovalent interactions for assembling metallacycles[32−36] and metallacages,[37−44] which are further employed as supramolecular hosts with predictable shapes and sizes. Compared with two-dimensional metallacycles, metallacages possess three-dimensional structures and cavities, making them encapsulate guest molecules from multiple directions and thus offering host–guest complexes with high binding affinities.[45,46] Therefore, during the past three decades, various metallacages have been extensively investigated and applied for guest encapsulation,[47−49] catalysis,[50−53] stabilizing reactive intermediates,[54,55] etc. Among them, porphyrin-based metallacages[56,57] have received much attention because they integrate the interesting optical and redox abilities of porphyrins and the host–guest properties of metallacages, offering extra functionalization such as light-harvesting and biological catalysis.[58−62] As an important branch of porphyrin-based metallacages, multicomponents have also been widely explored.[63−65] However, although these papers proposed that they had the metallacages, no crystal structures were provided. In a very recent study,[66] different from previously reported

Received: April 20, 2022
Revised: May 19, 2022
Accepted: May 20, 2022
Published: June 1, 2022

https://doi.org/10.1021/jacsau.2c00245
JACS Au 2022, 2, 1479–1487

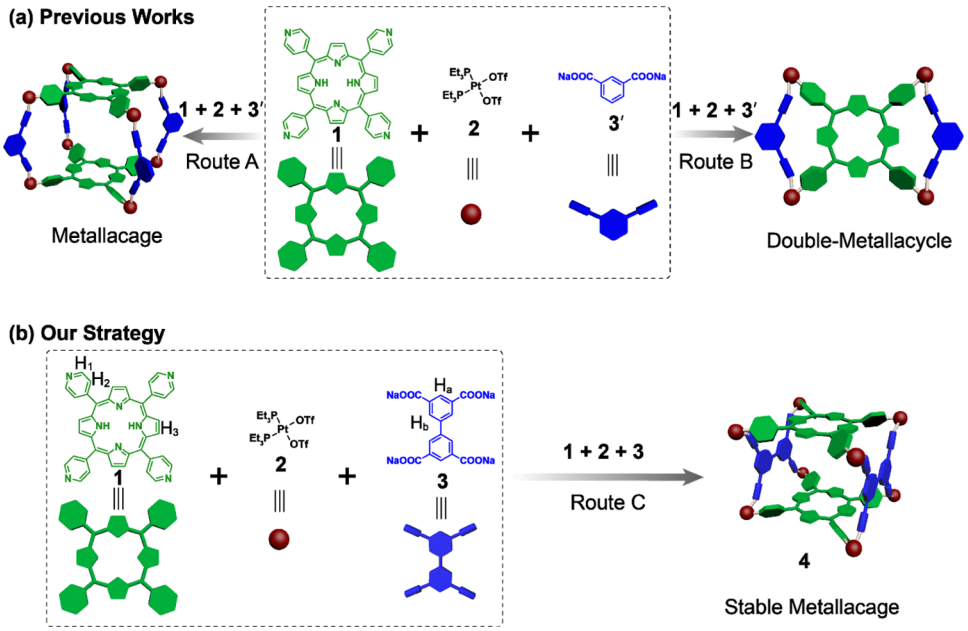

Figure 1. Different strategies for the self-assembly from tetrapyridyl porphyrin **1**, *cis*-Pt$(PEt_3)_2(OTf)_2$ **2**, and multicarboxylate ligands **3** or **3′**.

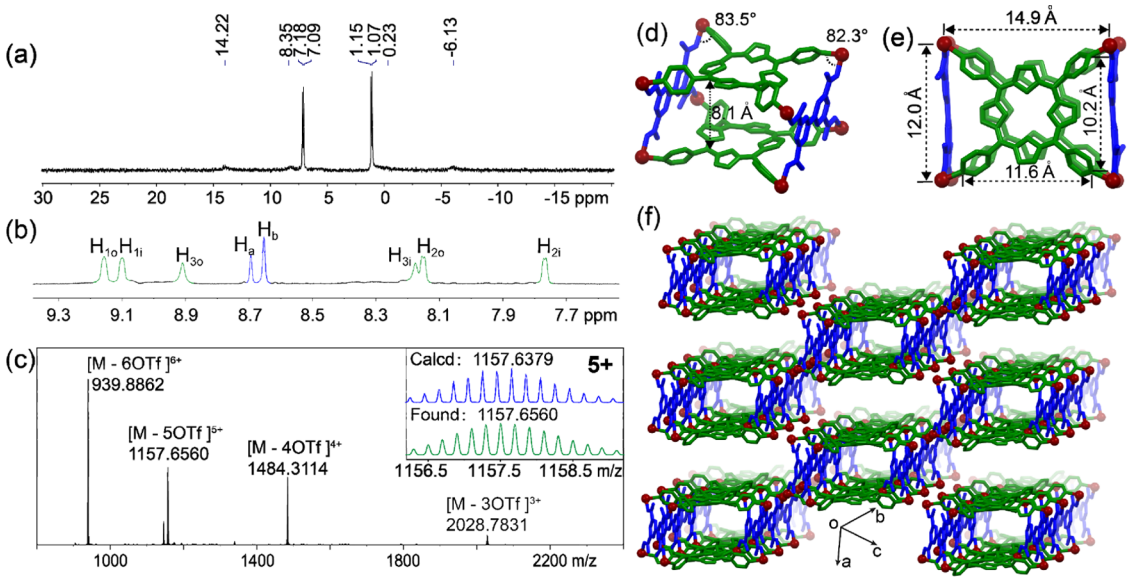

Figure 2. (a) Cartoon representations of metallacage **4** by multicomponent self-assembly; partial (b) ^{31}P $\{^1H\}$ and (c) ^1H NMR spectra (243 or 600 MHz, CD_3CN, 295 K) of metallacage **4**; (d) ESI-TOF-MS spectra of metallacage **4**. (d–f) Crystal structure of metallacage **4**. Hydrogen atoms, triethylphosphine units, counterions, and solvent molecules were omitted for clarity.[72]

three-dimensional (3D) prisms (Figure 1, route A), the self-assembly from tetrapyridyl porphyrin (**1**), Pt$(PEt_3)_2(OTf)_2$ (**2**), and dicarboxylate ligands (**3′**) was found to afford two-dimensional (2D) Bow Ties (Figure 1, route B) instead of 3D prisms, based on the X-ray crystal structures and detailed nuclear magnetic resonance (NMR) analysis. This finding casted a shadow on the future study of porphyrin-based multicomponent metallacages. Therefore, the exploration of multicomponent self-assembly to generate metallacages rather than metallacycles is urgently needed.

Herein, we use tetracarboxylate ligands (**3**) instead of dicarboxylate ligands (**3′**) as the carboxylic building blocks and prepare a porphyrin-based metallacage (**4**) via multicomponent self-assembly (Figure 1, route C). This strategy excludes the formation of 2D metallacycle structures and offers improved stability for the metallacage via multiple cooperative N–Pt–O coordination bonds. Moreover, the metallacage possesses a box-shaped structure with openings at both ends, which can allow easy access for planar organic molecules. The two π-conjugated, electron-rich porphyrin faces are aligned parallel to encapsulate planar molecules through π–π stacking. Therefore, the host–guest chemistry of the porphyrin-based metallacage was further systematically studied using polycyclic aromatic hydrocarbons (PAHs) as the guests.[67−71] It is worth mentioning that the crystal structures of all of the host–guest complexes are well resolved. More interestingly, the metallacage can generate singlet oxygen ($^1O_2$) effectively upon photoirradiation, which will weaken the host–guest interactions and trigger the release of anthracene-derived guests via photooxidation. By further heating the system, the released

https://doi.org/10.1021/jacsau.2c00245
JACS Au 2022, 2, 1479–1487

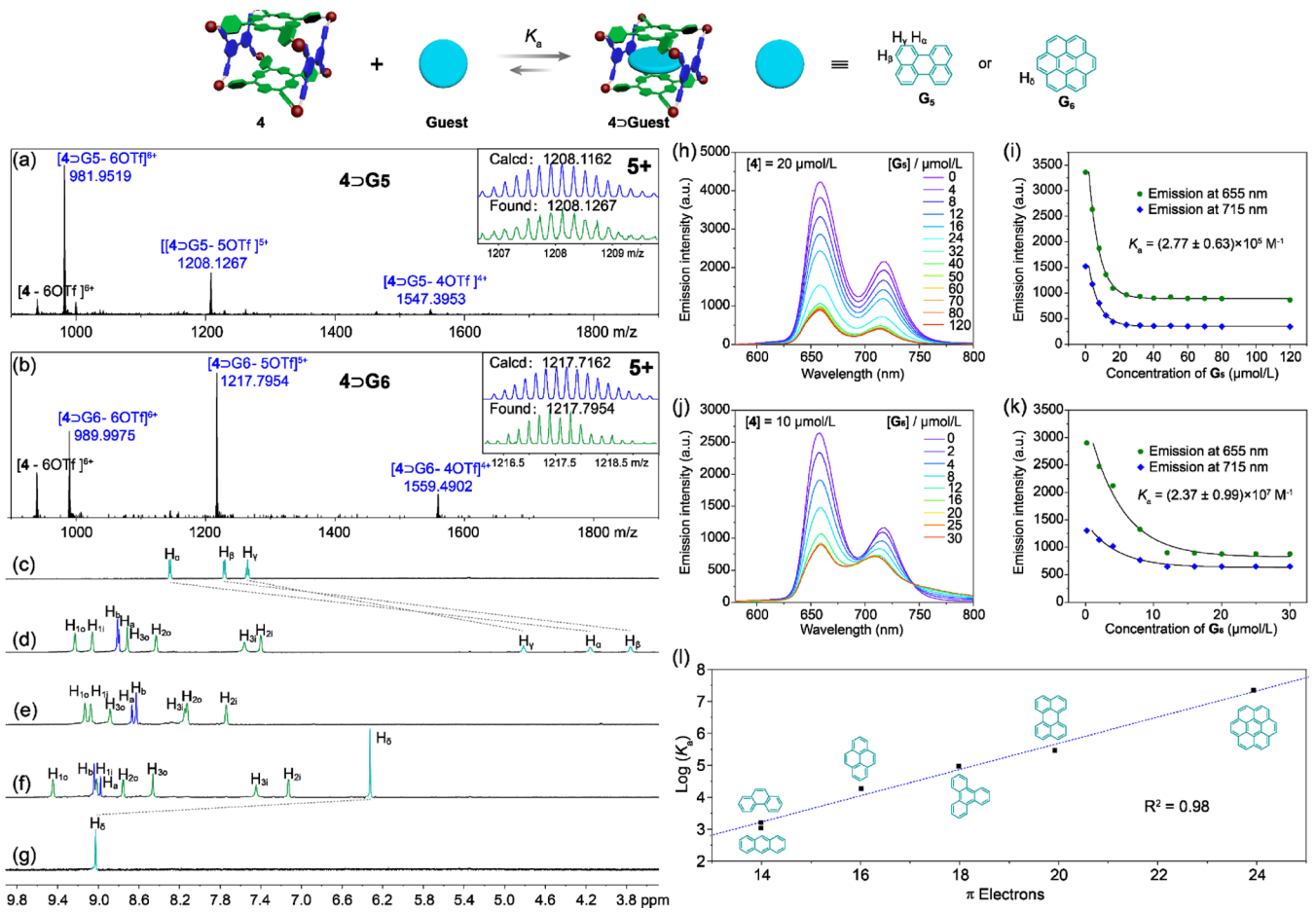

Figure 3. ESI-TOF-MS spectra of (a) **4**⊃$\mathbf{G_5}$ and (b) **4**⊃$\mathbf{G_6}$; partial ^{1}H NMR spectra (600 MHz, CD_3CN, 298 K) of (c) $\mathbf{G_5}$, (d) **4**⊃$\mathbf{G_5}$, (e) **4**, (f) **4**⊃$\mathbf{G_6}$, and (g) $\mathbf{G_6}$. [Host] = [Guest] = 1.00 mM. Fluorescence spectra of metallacage **4** at a fixed concentration upon the addition of (h) $\mathbf{G_5}$ and (j) $\mathbf{G_6}$ in $CH_3CN/CHCl_3$ (ν/ν = 9/1); nonlinear fitting curves of the emission intensity at 655 and 715 nm of metallacage **4** versus the concentrations of (i) $\mathbf{G_5}$ and (k) $\mathbf{G_6}$; and (l) plots of the logarithms of the association constants versus the number of π electrons on PAHs in $CH_3CN/CHCl_3$ (ν/ν = 9/1).

endoperoxide guest, viz., 10-phenyl-9-(2-phenylethynyl)-anthracene, can be converted back and reencapsulated. Such a host–guest system with photoresponsive encapsulation and release capability is constructed and may find further applications as stimuli-responsive materials.

RESULTS AND DISCUSSION

Preparation and Characterization Studies of Metallacages

Based on the self-assembly of tetrapyridyl porphyrin (**1**), tetracarboxylic ligand (**2**), and *cis*-Pt$(PEt_3)_2(OTf)_2$ (**3**), metallacage **4** was successfully prepared. The structure of the metallacage was fully characterized by multinuclear NMR ($^{31}P\{^1H\}$ and ^1H), electrospray ionization time-of-flight mass spectrometry (ESI-TOF-MS), and X-ray diffraction analysis. The $^{31}P\{^1H\}$ NMR spectra of **4** split into two doublet peaks at 7.14 and 1.11 ppm (Figure 2a), which hold equal intensities with concomitant ^{195}Pt satellites due to different phosphorus environments after the coordination of platinum atoms with pyridyl and carboxylic groups. In the ^1H NMR spectra (Figure 2b), diagnostic chemical shift changes were observed for the porphyrinic protons H_1, H_2, and H_3 and all of them split into two sets of signals after coordination, corresponding to the protons inside and outside of the metallacage. ESI-TOF-MS provided further evidence of the formation of the metallacage (Figure 2c). Peaks at m/z 939.8862, 1157.6560, 1484.3114, and 2028.7831 were found with isotopically well-resolved patterns, corresponding to $[\mathbf{4} - 6OTf]^{6+}$, $[\mathbf{4} - 5OTf]^{5+}$, $[\mathbf{4} - 4OTf]^{4+}$, and $[\mathbf{4} - 3OTf]^{3+}$.

Single crystals of **4** suitable for X-ray diffraction analysis were obtained by vapor diffusion of *i*-propyl ether into acetonitrile for 3 weeks. The crystal structure (Figures 2d–f, S5, and S6) provides direct evidence for the formation of the metallacage. To the best of our knowledge, this is the first time that the crystal structure of porphyrin-based multicomponent Pt(II)-metallacage is resolved.[63−65] The two porphyrinic and biphenyl units are connected by eight Pt atoms and the angles of N–Pt–O are 82.3–83.5°, forming a box-like metallacage with a dimension of 14.9 × 12.0 × 8.3 Å^3, based on the distance between the Pt atoms. The two porphyrin panels in the metallacage are parallel with each other and the distance between the two panels is 8.1 Å, which is an ideal distance to enable π–π stacking interactions with encapsulated aromatic guests. Moreover, this type of connection offers two large windows, which assist the guest molecules to enter into the cavity to form stable host–guest complexes. The metallacages are aligned along with the windows to form nanochannels (Figure 2f), which may facilitate host–guest complexation in the solid state.

https://doi.org/10.1021/jacsau.2c00245
JACS Au 2022, 2, 1479–1487

UV/vis and fluorescence spectra (Figure S7) of ligand **1** and metallacage **4** were further collected to study their photophysical properties. Ligand **1** and metallacage **4** showed a strong Soret peak centered at ca. 417 nm and four Q bands centered at ca. 650, 590, 550, and 515 nm, respectively, which are the typical absorption of porphyrin derivatives.[73] Two emission peaks at 655 and 717 nm were observed for **1** and **4**. Since porphyrin derivatives can generate singlet oxygen effectively upon photoirradiation,[74] the $^1O_2$ generation capabilities of **1** and **4** were studied by collecting the phosphorescence emission spectra of $^1O_2$. An intense peak at 1270 nm (Figure S8) was observed for both **1** and **4** upon irradiation (λ_{ex} = 405 nm), consisting of the photodegradation of 1,3-diphenylisobenzofuran using two photosensitizers (Figures S9 and S10), suggesting the strong $^1O_2$ generation ability of both the ligand and the metallacage.

Host–Guest Properties of Metallacage 4

Considering that metallacage **4** possesses a box-shaped cavity and two electron-rich porphyrin faces, its complexation with PAHs including anthracene ($\mathbf{G_1}$), phenanthrene ($\mathbf{G_2}$), pyrene ($\mathbf{G_3}$), triphenylene ($\mathbf{G_4}$), perylene ($\mathbf{G_5}$), and coronene ($\mathbf{G_6}$) was further studied. Taking coronene as an example, when it was added to the acetonitrile solution of **4**, a color change from claret-red to brown was observed, suggesting the charge-transfer interactions between **4** and $\mathbf{G_6}$. Job's plots based on UV/vis spectroscopic absorbance data (λ = 417 nm) were carried out, indicating that the complexes of **4** with PAHs in acetonitrile were all of 1:1 stoichiometries (Figures S11–S16). This was also confirmed by ESI-TOF-MS (Figures 3a,b and S17). For example, peaks were observed at m/z 989.9975, 1217.7954, and 1559.4902 (Figure 3b), corresponding to $[\mathbf{4}\supset\mathbf{G_6} - 6\mathrm{OTf}]^{6+}$, $[\mathbf{4}\supset\mathbf{G_6} - 5\mathrm{OTf}]^{5+}$, and $[\mathbf{4}\supset\mathbf{G_6} - 4\mathrm{OTf}]^{4+}$. The complexation between metallacage **4** and PAHs was further studied by ^{1}H NMR spectroscopy (Figures 3c–g and S18–S23). All complexation systems exhibit fast exchange on the proton NMR timescale because the large windows of the metallacage make it easy for the guests to get in and out. Significant upfield shifts were observed for all of the resonances of the bound guests, indicating good host–guest interactions. For example, protons H_α, H_β, and H_γ of $\mathbf{G_5}$ and proton H_δ of $\mathbf{G_6}$ shifted from 8.30, 7.76, 7.53, and 9.03 ppm to 4.16, 3.76, 4.81, and 6.32 ppm, respectively. Correspondingly, all of the resonances of metallacage **4** undergo significant changes with downfield or upfield shifts. These results indicated that the cavity of **4** provided a shielded magnetic environment for the guests.

Concentration-dependent fluorescence titration experiments were carried out to measure the association constants (K_a) between metallacage **4** and PAHs in solution. For a better comparison, $CH_3CN/CHCl_3$ (ν/ν = 9/1) was used as the solvent owing to the poor solubility of large PAHs such as perylene and coronene in acetonitrile. The fluorescence intensity of metallacage **4** decreased gradually upon the addition of the guests. The K_a of $\mathbf{4}\supset\mathbf{G_1}$, $\mathbf{4}\supset\mathbf{G_2}$, $\mathbf{4}\supset\mathbf{G_3}$, $\mathbf{4}\supset\mathbf{G_4}$, $\mathbf{4}\supset\mathbf{G_5}$, and $\mathbf{4}\supset\mathbf{G_6}$ were determined as $(1.19 \pm 0.06) \times 10^3$, $(1.55 \pm 0.04) \times 10^3$, $(1.94 \pm 0.09) \times 10^4$, $(9.33 \pm 0.74) \times 10^4$, $(2.77 \pm 0.63) \times 10^5$, and $(2.37 \pm 0.99) \times 10^7$ M^{-1}, respectively (Figures 3h–l and S28–S33). It is worth noting that these values are among the highest binding constants for metallacage-based host–guest complexes.[46,75] This is because the two porphyrin faces in the metallacage are well organized in an ideal distance to promote the π–π stacking interactions with encapsulated PAHs. Interestingly, the values of log K_a are linearly proportional to the number of π-electrons on PAHs (Figure 3l and Table 1) with a correlation coefficient of 0.98. This could be used to predict the association constants between metallacage and PAHs.

Table 1. Association Constants between Metallacage 4 and Different PAHs

guest molecules	number of π electrons	association constant (K_a, M^{-1})	
		CH_3CN	$CH_3CN/CHCl_3$ (ν/ν = 9/1)
$\mathbf{G_1}$	14	$(4.72 \pm 0.11) \times 10^3$	$(1.19 \pm 0.6) \times 10^3$
$\mathbf{G_2}$	14	$(9.05 \pm 0.27) \times 10^3$	$(1.55 \pm 0.04) \times 10^3$
$\mathbf{G_3}$	16	$(9.37 \pm 1.67) \times 10^4$	$(1.94 \pm 0.09) \times 10^4$
$\mathbf{G_4}$	18	$(6.66 \pm 3.53) \times 10^5$	$(9.33 \pm 0.74) \times 10^4$
$\mathbf{G_5}$	20		$(2.77 \pm 0.63) \times 10^5$
$\mathbf{G_6}$	24		$(2.37 \pm 0.99) \times 10^7$

The single crystals of metallacage **4** with a series of PAHs suitable for X-ray diffraction analysis were also obtained by vapor diffusion of *i*-propyl ether into acetonitrile for 3 weeks and provided unambiguous evidence for the formation of inclusion complexes. Ranging from three to seven fused benzenoid rings, the crystalline complexes (Figure 4) formed between metallacage **4** and various PAHs with a 1:1 stoichiometry were isolated. It is worth mentioning that the distance between the two porphyrin faces decreased from ca. 8.1 to 7.0 Å after complexation. Correspondingly, the distances between the PAHs and porphyrin faces are 3.4–3.6 Å, which meets the requirements for π–π stacking interactions. It can be seen from the top views of crystal structures (Figure 4) that the PAHs align themselves in register with the maximum number of binding sites in metallacage **4** by translational positioning or rotational location. In the crystal structures, anthracene, phenanthrene, pyrene, and triphenylene are disordered, leading to the broad signals of the protons on these guests in the ^{1}H NMR spectra (Figures S18–S21) after complexation. However, for perylene and coronene, extra [C–H···π] interactions were also found between their peripheral protons and the phenyl rings of the carboxylic ligands to stabilize the whole complexes in addition to the π–π stacking interactions (Figure 4m,n). Therefore, the movements of perylene or coronene inside the cavity are restricted, giving sharp signals of the guests in the ^{1}H NMR spectra (Figures 3c–g, S22, and S23).

Photooxidation-Triggered Encapsulation and Release

The stimuli responsiveness of such host–guest complexation was further explored. As the metallacage can generate $^1O_2$ effectively, the oxidation of anthracene inside the metallacage was conducted (Figure 5a–d). The encapsulated anthracene fully converted into epidioxyanthracene upon photoirradiation (λ_{ex} = 405 nm) for 10 min, as revealed from the fact that all of the peaks of the protons for anthracene disappeared and the peaks of the protons for epidioxyanthracene emerged (Figure 5b,c). It is worth mentioning that the chemical shifts of the epidioxyanthracene protons located at the same position with free epidioxyanthracene (Figure 5c,d), suggesting that epidioxyanthracene was released from the cavity of the metallacage after oxidation. This was also evidenced by the DOSY experiments (Figures S34 and S35) that epidioxyanthracene showed a different diffusion coefficient ($D = 2.31 \times 10^{-9}$ m^2 s^{-1}) from that of metallacage **4** ($D = 6.21 \times 10^{-10}$ m^2

https://doi.org/10.1021/jacsau.2c00245
JACS Au 2022, 2, 1479–1487

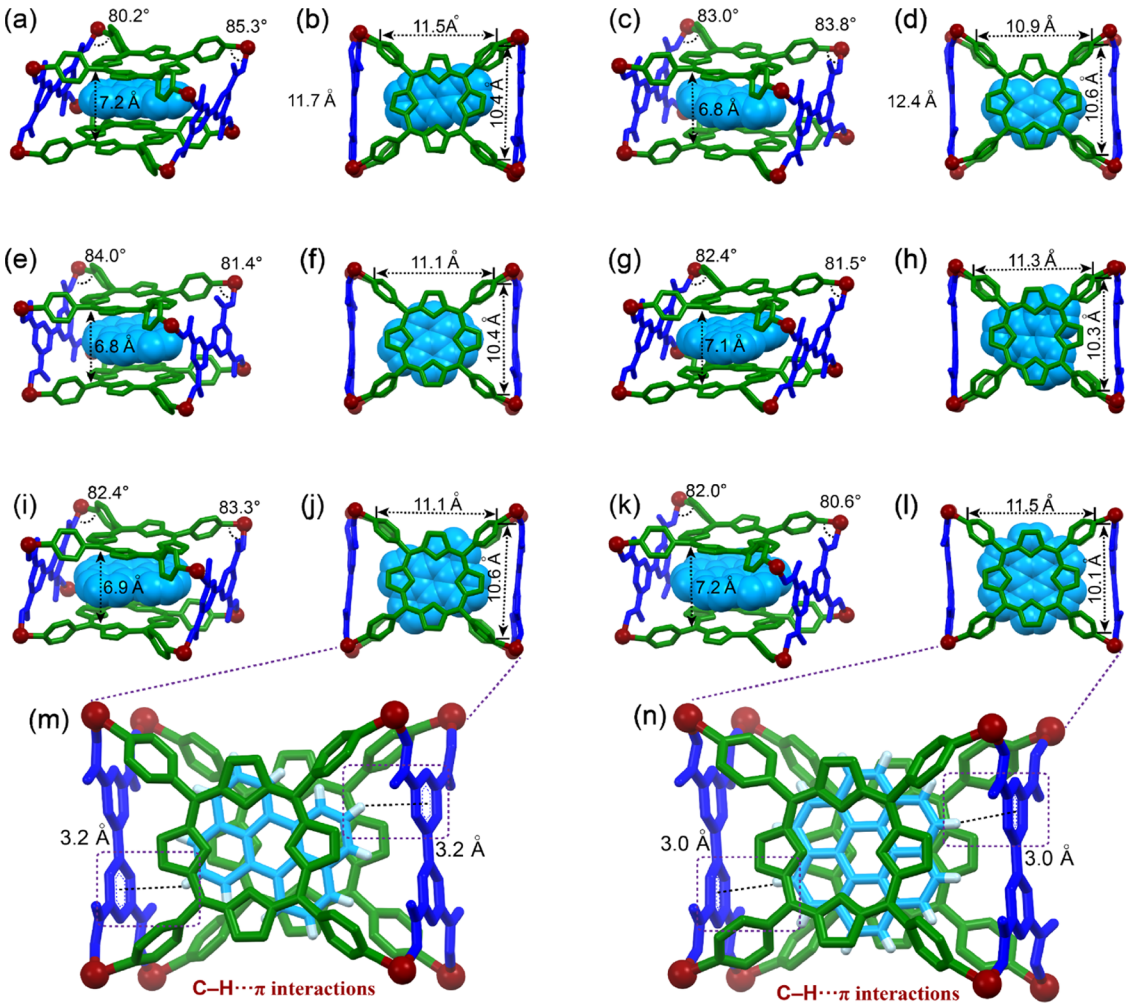

Figure 4. Crystal structures of (a, b) **4**⊃$\mathbf{G_1}$, (c, d) **4**⊃$\mathbf{G_2}$, (e, f) **4**⊃$\mathbf{G_3}$, (g, h) **4**⊃$\mathbf{G_4}$, (i, j, m) **4**⊃$\mathbf{G_5}$, and (k, l, n) **4**⊃$\mathbf{G_6}$. Hydrogen atoms, triethylphosphine units, counterions, and solvent molecules were omitted for clarity.[72]

s^{-1}), while the complex **4**⊃anthracene only exhibits one single diffusion coefficient (D = 6.55 × 10^{-10} m^2 s^{-1}). However, epidioxyanthracene would decompose upon heating,[76] so the reencapsulation process cannot take place using anthracene as the guest.

To construct a reversible photooxidation-triggered host–guest complexation, we screened several anthracene derivatives (Figure 5e) to find a suitable guest for the metallacage. Compounds $\mathbf{G_7}$, $\mathbf{G_8}$, and $\mathbf{G_9}$ showed good host–guest interactions with metallacage **4** (Figures S41–S44). Compounds $\mathbf{G_7}$ and $\mathbf{G_8}$ could be converted into their epidioxyanthracene analogues upon irradiation at 405 nm. However, their endoperoxides would undergo fast deoxidation to their original structures at room temperature. The encapsulated $\mathbf{G_9}$ failed to be converted into its endoperoxide upon irradiation, owing to its high stability. Due to steric hindrance of the benzene rings on both sides, $\mathbf{G_{10}}$ showed a poor host–guest interaction with metallacage **4** (Figure S45). Therefore, 10-phenyl-9-(2-phenylethynyl)anthracene ($\mathbf{G_{11}}$) was chosen as the guest for the construction of this reversible host–guest complex because its endoperoxide $\mathbf{G_{11}}$–$\mathbf{O_2}$ showed moderate stability at room temperature and could be converted back to $\mathbf{G_{11}}$ upon heating quickly (Figures S46 and S51).[77]

Compound $\mathbf{G_{11}}$ also formed stable 1:1 host–guest complexes (Figure S46) with metallacage **4**. This was confirmed by ESI-TOF-MS as well (Figure S46c). Peaks were observed at m/z 998.3403, 1227.8087, 1572.0200, and 2145.6626, corresponding to $[\mathbf{4}\supset\mathbf{G_{11}} - 6\mathrm{OTf}]^{6+}$, $[\mathbf{4}\supset\mathbf{G_{11}} - 5\mathrm{OTf}]^{5+}$, $[\mathbf{4}\supset\mathbf{G_{11}} - 4\mathrm{OTf}]^{4+}$, and $[\mathbf{4}\supset\mathbf{G_{11}} - 3\mathrm{OTf}]^{3+}$. Single crystals of metallacage **4** with $\mathbf{G_{11}}$ suitable for X-ray diffraction analysis were also obtained and provided unambiguous evidence for the formation of inclusion complex **4**⊃$\mathbf{G_{11}}$ with a 1:1 stoichiometry (Figure S46d,e). The K_a of **4**⊃$\mathbf{G_{11}}$ was determined to be (5.48 ± 0.31) × 10^3 M^{-1} (Figures S49 and S50), which was similar to that of **4**⊃$\mathbf{G_1}$ in acetonitrile. When complex **4**⊃$\mathbf{G_{11}}$ was irradiated for 20 min (λ_{ex} = 405 nm, Figure 5f–i) in air at atmospheric pressure, $^1O_2$ generated by the metallacage converted $\mathbf{G_{11}}$ into $\mathbf{G_{11}}$–$\mathbf{O_2}$ completely, leading to the release of the guest from its cavity. Upon heating at 80 °C for 30 min, $\mathbf{G_{11}}$–$\mathbf{O_2}$ was transferred back into G_{11} and the host–guest complex **4**⊃$\mathbf{G_{11}}$ formed again (Figure 5h,i). These processes were also confirmed by the fluorescence experiments. The emission intensity at 470 nm derived from compound $\mathbf{G_{11}}$ decreased gradually upon photoirradiation, while the emission band at 660 nm ascribed to metallacage **4** was almost constant, suggesting the transformation of $\mathbf{G_{11}}$ into its endoperoxide (Figure 5j). After heating, the emission of the solution was restored to its initial value (Figure S51). This process is fully reversible and could be repeated at least five times with a good fatigue resistance (Figure 5k). Therefore,

https://doi.org/10.1021/jacsau.2c00245
JACS Au 2022, 2, 1479–1487

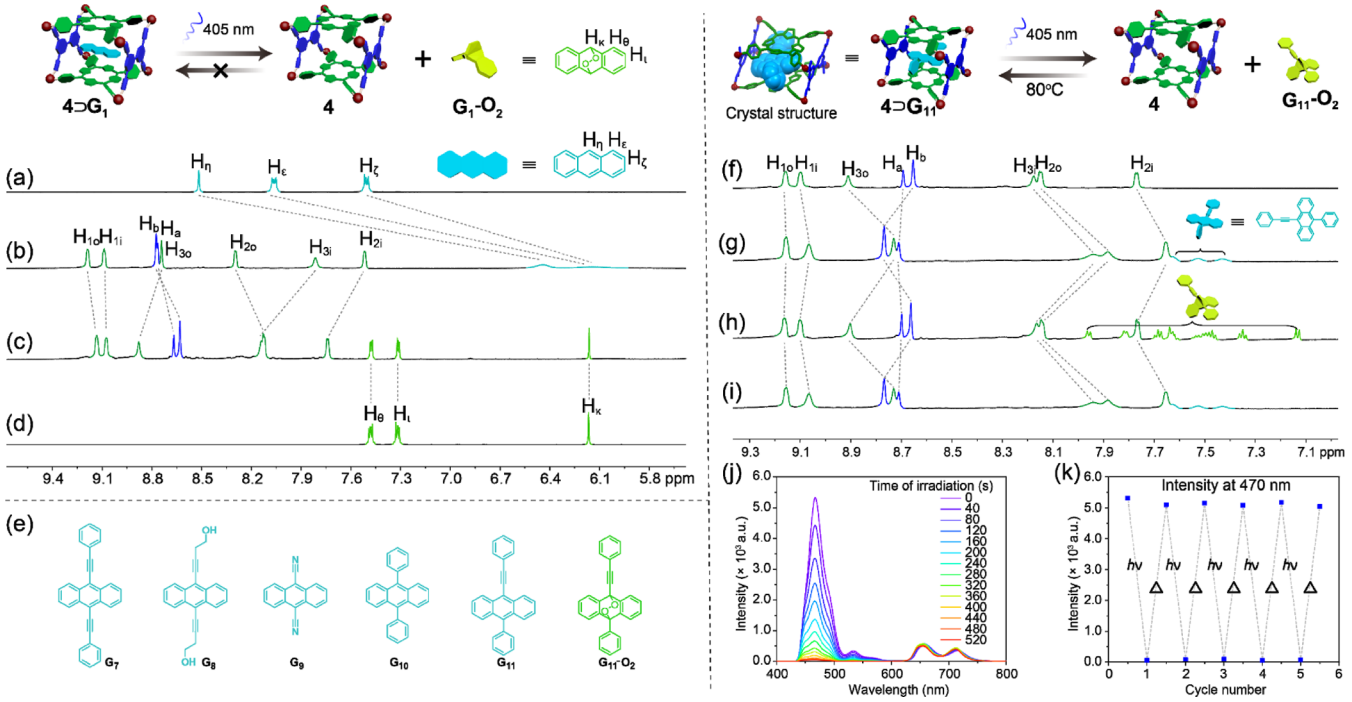

Figure 5. Partial ^{1}H NMR spectra (600 MHz, CD_3CN, 295 K) of (a) $\mathbf{G_1}$, (b) $\mathbf{4}\supset\mathbf{G_1}$, and (c) $\mathbf{4}\supset\mathbf{G_1}$ upon photoirradiation for 10 min and (d) epidioxyanthracene $\mathbf{G_1}$–$\mathbf{O_2}$. (e) Chemical structures of anthracene derivatives tested in the reversible controlled release study. Partial ^{1}H NMR spectra (600 MHz, CD_3CN, 295 K) of (f) **4**, (g) $\mathbf{4}\supset\mathbf{G_{11}}$, and (h) $\mathbf{4}\supset\mathbf{G_{11}}$ upon photoirradiation for 20 min, (i) and heating at 80°C for 30 min. (j, k) Fatigue cycles for the reversible host–guest system characterized by fluorescence spectroscopy. [Host] = [Guest] = 10.00 M, λ_{ex} = 405 nm.

photooxidation-triggered reversible host–guest complexation was successfully prepared, which holds great potential for the construction of photoresponsive smart materials.

CONCLUSIONS

In summary, a box-shaped porphyrin-based metallacage was prepared by a multicomponent coordination-driven self-assembly. Owing to its electron-rich planar porphyrin face and suitable cavity size, the metallacage showed enhanced host–guest interactions with a series of PAHs. It was further employed to construct a reversible photoresponsive host–guest complexation system based on the photooxidation-triggered release of anthracene derivatives and the reencapsulation of guests upon heating. Our ongoing study reveals that different metalloporphyrins can also be introduced for the construction of such metallacages, suggesting the versatility of the multicomponent strategy in the construction of barrel-shaped metallacages. We believe that our current study offers a photoresponsive host–guest system, which is driven by the structural changes of guest molecules via photooxidation, which will guide the future design and applications of metallacages for stimuli-responsive materials.

ASSOCIATED CONTENT

Supporting Information

The Supporting Information is available free of charge at https://pubs.acs.org/doi/10.1021/jacsau.2c00245.

Experimental details and characterization, spectra (^{1}H NMR, ^{13}C NMR, ESI-MS spectra, UV–vis absorption, and fluorescence spectra) (PDF)
Crystal diffraction data for **4** (CIF)
Crystal diffraction data for $\mathbf{4}\supset\mathbf{G_1}$ (CIF)
Crystal diffraction data for $\mathbf{4}\supset\mathbf{G_2}$ (CIF)
Crystal diffraction data for $\mathbf{4}\supset\mathbf{G_3}$ (CIF)
Crystal diffraction data for $\mathbf{4}\supset\mathbf{G_4}$ (CIF)
Crystal diffraction data for $\mathbf{4}\supset\mathbf{G_5}$ (CIF)
Crystal diffraction data for $\mathbf{4}\supset\mathbf{G_6}$ (CIF)
Crystal diffraction data for $\mathbf{4}\supset\mathbf{G_{11}}$ (CIF)

AUTHOR INFORMATION

Corresponding Author

Mingming Zhang – *State Key Laboratory for Mechanical Behavior of Materials, Shaanxi International Research Center for Soft Matter, School of Materials Science and Engineering, Xi'an Jiaotong University, Xi'an 710049, P. R. China;* orcid.org/0000-0003-3156-7811; Email: mingming.zhang@xjtu.edu.cn

Authors

Zeyuan Zhang – *State Key Laboratory for Mechanical Behavior of Materials, Shaanxi International Research Center for Soft Matter, School of Materials Science and Engineering, Xi'an Jiaotong University, Xi'an 710049, P. R. China*

Lingzhi Ma – *State Key Laboratory for Mechanical Behavior of Materials, Shaanxi International Research Center for Soft Matter, School of Materials Science and Engineering, Xi'an Jiaotong University, Xi'an 710049, P. R. China*

Fang Fang – *Instrumental Analysis Center of Shenzhen University, Shenzhen 518055, P. R. China*

Yali Hou – *State Key Laboratory for Mechanical Behavior of Materials, Shaanxi International Research Center for Soft Matter, School of Materials Science and Engineering, Xi'an Jiaotong University, Xi'an 710049, P. R. China*

Chenjie Lu – *Key Laboratory of Adsorption and Separation Materials and Technologies of Zhejiang Province, Zhejiang University, Hangzhou 310027, P. R. China*

https://doi.org/10.1021/jacsau.2c00245
JACS Au 2022, 2, 1479–1487

Chaoqun Mu − *State Key Laboratory for Mechanical Behavior of Materials, Shaanxi International Research Center for Soft Matter, School of Materials Science and Engineering, Xi'an Jiaotong University, Xi'an 710049, P. R. China*
Yafei Zhang − *State Key Laboratory for Mechanical Behavior of Materials, Shaanxi International Research Center for Soft Matter, School of Materials Science and Engineering, Xi'an Jiaotong University, Xi'an 710049, P. R. China*
Haifei Liu − *State Key Laboratory for Mechanical Behavior of Materials, Shaanxi International Research Center for Soft Matter, School of Materials Science and Engineering, Xi'an Jiaotong University, Xi'an 710049, P. R. China*
Ke Gao − *State Key Laboratory for Mechanical Behavior of Materials, Shaanxi International Research Center for Soft Matter, School of Materials Science and Engineering, Xi'an Jiaotong University, Xi'an 710049, P. R. China*
Ming Wang − *State Key Laboratory of Supramolecular Structure and Materials, College of Chemistry, Jilin University, Changchun 130012, P. R. China;* orcid.org/0000-0002-5332-0804
Zixi Zhang − *Department of Dermatology, The First Affiliated Hospital of Xi'an Jiaotong University, Xi'an 710061, P. R. China*
Xiaopeng Li − *College of Chemistry and Environmental Engineering, Shenzhen University, Shenzhen 518055, P. R. China;* orcid.org/0000-0001-9655-9551

Complete contact information is available at: https://pubs.acs.org/10.1021/jacsau.2c00245

Funding

This work was supported by the National Natural Science Foundation of China (22171219 to M.Z.), the Open Project of State Key Laboratory of Supramolecular Structure and Materials (sklssm2021033), and the Fundamental Research Funds for the Central Universities.

Notes

The authors declare no competing financial interest.

■ ACKNOWLEDGMENTS

The authors thank Dr. Gang Chang and Yu Wang at the Instrument Analysis Center and Dr. Aqun Zheng and Junjie Zhang at the Experimental Chemistry Center of Xi'an Jiaotong University for NMR and fluorescence measurements. The authors also acknowledge the mass spectrometry characterization by the Molecular Scale Laboratory.

■ REFERENCES

(1) Huang, F.; Anslyn, E. V. Introduction: Supramolecular Chemistry. *Chem. Rev.* **2015**, *115*, 6999−7000.
(2) Liu, Z.; Nalluri, S. K. M.; Stoddart, J. F. Surveying Macrocyclic Chemistry: From Flexible Crown Ethers to Rigid Cyclophanes. *Chem. Soc. Rev.* **2017**, *46*, 2459−2478.
(3) Xia, D.; Wang, P.; Ji, X.; Khashab, N. M.; Sessler, J. L.; Huang, F. Functional Supramolecular Polymeric Networks: The Marriage of Covalent Polymers and Macrocycle-Based Host-Guest Interactions. *Chem. Rev.* **2020**, *120*, 6070−6123.
(4) Beatty, M. A.; Hof, F. Host−Guest Binding in Water, Salty Water, and Biofluids: General Lessons for Synthetic, Bio-targeted Molecular Recognition. *Chem. Soc. Rev.* **2021**, *50*, 4812−4832.
(5) Pedersen, C. J. Cyclic Polyethers and Their Complexes with Metal Salts. *J. Am. Chem. Soc.* **1967**, *89*, 7017−7036.
(6) Lehn, J. M. Cryptates: The Chemistry of Macropolycyclic Inclusion Complexes. *Acc. Chem. Res.* **1978**, *11*, 49−57.
(7) He, Q.; Vargas-Zúñiga, G. I.; Kim, S. H.; Kim, S. K.; Sessler, J. L. Macrocycles as Ion Pair Receptors. *Chem. Rev.* **2019**, *119*, 9753−9835.
(8) Prochowicz, D.; Kornowicz, A.; Lewiński, J. Interactions of Native Cyclodextrins with Metal Ions and Inorganic Nanoparticles: Fertile Landscape for Chemistry and Materials Science. *Chem. Rev.* **2017**, *117*, 13461−13501.
(9) Roy, I.; Stoddart, J. F. Cyclodextrin Metal−Organic Frameworks and Their Applications. *Acc. Chem. Res.* **2021**, *54*, 1440−1453.
(10) Guo, D.-S.; Liu, Y. Supramolecular Chemistry of *p*-Sulfonatocalix[*n*]arenes and Its Biological Applications. *Acc. Chem. Res.* **2014**, *47*, 1925−1934.
(11) Kumar, R.; Sharma, A.; Singh, H.; Suating, P.; Kim, H. S.; Sunwoo, K.; Shim, I.; Gibb, B. C.; Kim, J. S. Revisiting Fluorescent Calixarenes: from Molecular Sensors to Smart Materials. *Chem. Rev.* **2019**, *119*, 9657−9721.
(12) Barrow, S. J.; Kasera, S.; Rowland, M. J.; Del Barrio, J.; Scherman, O. A. Cucurbituril-Based Molecular Recognition. *Chem. Rev.* **2015**, *115*, 12320−12406.
(13) Murray, J.; Kim, K.; Ogoshi, T.; Yao, W.; Gibb, B. C. The Aqueous Supramolecular Chemistry of Cucurbit[*n*]urils, Pillar[*n*]-arenes and Deep-Cavity Cavitands. *Chem. Soc. Rev.* **2017**, *46*, 2479−2496.
(14) Dale, E. J.; Vermeulen, N. A.; Juricek, M.; Barnes, J. C.; Young, R. M.; Wasielewski, M. R.; Stoddart, J. F. Supramolecular Explorations: Exhibiting the Extent of Extended Cationic Cyclophanes. *Acc. Chem. Res.* **2016**, *49*, 262−273.
(15) Cai, K.; Zhang, L.; Astumian, R. D.; Stoddart, J. F. Radical-Pairing-Induced Molecular Assembly and Motion. *Nat. Rev. Chem.* **2021**, *5*, 447−465.
(16) Ogoshi, T.; Yamagishi, T.; Nakamoto, Y. Pillar-Shaped Macrocyclic Hosts Pillar[*n*]arenes: New Key Players for Supramolecular Chemistry. *Chem. Rev.* **2016**, *116*, 7937−8002.
(17) Fa, S.; Kakuta, T.; Yamagishi, T.-a.; Ogoshi, T. One-, Two-, and Three-Dimensional Supramolecular Assemblies Based on Tubular and Regular Polygonal Structures of Pillar[n]arenes. *CCS Chem.* **2019**, *1*, 50−63.
(18) You, L.; Zha, D.; Anslyn, E. V. Recent Advances in Supramolecular Analytical Chemistry Using Optical Sensing. *Chem. Rev.* **2015**, *115*, 7840−7892.
(19) Mako, T. L.; Racicot, J. M.; Levine, M. Supramolecular Luminescent Sensors. *Chem. Rev.* **2019**, *119*, 322−477.
(20) Wu, J. R.; Yang, Y. W. Synthetic Macrocycle-Based Nonporous Adaptive Crystals for Molecular Separation. *Angew. Chem., Int. Ed.* **2021**, *60*, 1690−1701.
(21) Shaffer, C. C.; Smith, B. D. Macrocyclic and Acyclic Supramolecular Elements for Co-precipitation of Square-Planar Gold(iii) Tetrahalide Complexes. *Org. Chem. Front.* **2021**, *8*, 1294−1301.
(22) Si, W.; Xin, P.; Li, Z.-T.; Hou, J.-L. Tubular Unimolecular Transmembrane Channels: Construction Strategy and Transport Activities. *Acc. Chem. Res.* **2015**, *48*, 1612−1619.
(23) Barboiu, M. Encapsulation versus Self-Aggregation toward Highly Selective Artificial K^+ Channels. *Acc. Chem. Res.* **2018**, *51*, 2711−2718.
(24) Webber, M. J.; Langer, R. Drug Delivery by Supramolecular Design. *Chem. Soc. Rev.* **2017**, *46*, 6600−6620.
(25) Omoto, K.; Tashiro, S.; Shionoya, M. Phase-Dependent Reactivity and Host-Guest Behaviors of a Metallo-Macrocycle in Liquid and Solid-State Photosensitized Oxygenation Reactions. *J. Am. Chem. Soc.* **2021**, *143*, 5406−5412.
(26) Vinciguerra, B.; Cao, L.; Cannon, J. R.; Zavalij, P. Y.; Fenselau, C.; Isaacs, L. Synthesis and Self-Assembly Processes of Monofunctionalized Cucurbit[7]uril. *J. Am. Chem. Soc.* **2012**, *134*, 13133−13140.
(27) Cao, L.; Hettiarachchi, G.; Briken, V.; Isaacs, L. Cucurbit[7]uril Containers for Targeted Delivery of Oxaliplatin to Cancer Cells. *Angew. Chem., Int. Ed.* **2013**, *52*, 12033−12037.

(28) Cook, T. R.; Stang, P. J. Recent Developments in the Preparation and Chemistry of Metallacycles and Metallacages via Coordination. *Chem. Rev.* **2015**, *115*, 7001−7045.
(29) Roberts, D. A.; Pilgrim, B. S.; Nitschke, J. R. Covalent Post-Assembly Modification in Metallosupramolecular Chemistry. *Chem. Soc. Rev.* **2018**, *47*, 626−644.
(30) Chen, L. J.; Yang, H. B. Construction of Stimuli-Responsive Functional Materials via Hierarchical Self-Assembly Involving Coordination Interactions. *Acc. Chem. Res.* **2018**, *51*, 2699−2710.
(31) Sun, Y.; Chen, C.; Liu, J.; Stang, P. J. Recent Developments in the Construction and Applications of Platinum-Based Metallacycles and Metallacages via Coordination. *Chem. Soc. Rev.* **2020**, *49*, 3889−3919.
(32) Chen, L. J.; Chen, S.; Qin, Y.; Xu, L.; Yin, G. Q.; Zhu, J. L.; Zhu, F. F.; Zheng, W.; Li, X.; Yang, H. B. Construction of Porphyrin-Containing Metallacycle with Improved Stability and Activity within Mesoporous Carbon. *J. Am. Chem. Soc.* **2018**, *140*, 5049−5052.
(33) Chen, L.; Chen, C.; Sun, Y.; Lu, S.; Huo, H.; Tan, T.; Li, A.; Li, X.; Ungar, G.; Liu, F.; Zhang, M. Luminescent Metallacycle-Cored Liquid Crystals Induced by Metal Coordination. *Angew. Chem., Int. Ed.* **2020**, *59*, 10143−10150.
(34) Jeyakkumar, P.; Liang, Y.; Guo, M.; Lu, S.; Xu, D.; Li, X.; Guo, B.; He, G.; Chu, D.; Zhang, M. Emissive Metallacycle-Crosslinked Supramolecular Networks with Tunable Crosslinking Densities for Bacterial Imaging and Killing. *Angew. Chem., Int. Ed.* **2020**, *59*, 15199−15203.
(35) Huang, B.; Liu, X.; Yang, G.; Tian, J.; Liu, Z.; Zhu, Y.; Li, X.; Yin, G.; Zheng, W.; Xu, L.; Zhang, W. A Near-Infrared Organoplatinum(II) Metallacycle Conjugated with Heptamethine Cyanine for Trimodal Cancer Therapy. *CCS Chem.* **2021**, *3*, 2055−2066.
(36) Sun, Y.; Tuo, W.; Stang, P. J. Metal-Organic Cycle-Based Multistage Assemblies. *Proc. Natl. Acad. Sci. U.S.A.* **2022**, *119*, No. e2122398119.
(37) Inokuma, Y.; Kawano, M.; Fujita, M. Crystalline Molecular Flasks. *Nat. Chem.* **2011**, *3*, 349−358.
(38) Brown, C. J.; Toste, F. D.; Bergman, R. G.; Raymond, K. N. Supramolecular Catalysis in Metal-Ligand cluster Hosts. *Chem. Rev.* **2015**, *115*, 3012−3035.
(39) Li, M.; Jiang, S.; Zhang, Z.; Hao, X.-Q.; Jiang, X.; Yu, H.; Wang, P.; Xu, B.; Wang, M.; Tian, W. Tetraphenylethylene-Based Emissive Supramolecular Metallacages Assembled by Terpyridine Ligands. *CCS Chem.* **2020**, *2*, 337−348.
(40) Zhang, Z.; Zhao, Z.; Hou, Y.; Wang, H.; Li, X.; He, G.; Zhang, M. Aqueous Platinum(II)-Cage-Based Light-Harvesting System for Photocatalytic Cross-Coupling Hydrogen Evolution Reaction. *Angew. Chem., Int. Ed.* **2019**, *58*, 8862−8866.
(41) Hou, Y.; Zhang, Z.; Lu, S.; Yuan, J.; Zhu, Q.; Chen, W.-P.; Ling, S.; Li, X.; Zheng, Y.-Z.; Zhu, K.; Zhang, M. Highly Emissive Perylene Diimide-Based Metallacages and Their Host-Guest Chemistry for Information Encryption. *J. Am. Chem. Soc.* **2020**, *142*, 18763−18768.
(42) Zhang, Z.; Zhao, Z.; Wu, L.; Lu, S.; Ling, S.; Li, G.; Xu, L.; Ma, L.; Hou, Y.; Wang, X.; Li, X.; He, G.; Wang, K.; Zou, B.; Zhang, M. Emissive Platinum(II) Cages with Reverse Fluorescence Resonance Energy Transfer for Multiple Sensing. *J. Am. Chem. Soc.* **2020**, *142*, 2592−2600.
(43) Hou, Y.; Zhang, Z.; Ma, L.; Shi, R.; Ling, S.; Li, X.; He, G.; Zhang, M. Perylene Diimide-Based Multicomponent Metallacages as Photosensitizers for Visible Light-Driven Photocatalytic Oxidation Reaction. *CCS Chem.* **2021**, 3153−3160.
(44) Mu, C.; Zhang, Z.; Hou, Y.; Liu, H.; Ma, L.; Li, X.; Ling, S.; He, G.; Zhang, M. Tetraphenylethylene-Based Multicomponent Emissive Metallacages as Solid-State Fluorescent Materials. *Angew. Chem., Int. Ed.* **2021**, *60*, 12293−12297.
(45) Nakamura, T.; Ube, H.; Shionoya, M. Silver-Mediated Formation of a Cofacial Porphyrin Dimer with the Ability to Intercalate Aromatic Molecules. *Angew. Chem., Int. Ed.* **2013**, *52*, 12096−12100.
(46) August, D. P.; Nichol, G. S.; Lusby, P. J. Maximizing Coordination Capsule-Guest Polar Interactions in Apolar Solvents Reveals Significant Binding. *Angew. Chem., Int. Ed.* **2016**, *55*, 15022−15026.
(47) Ibáñez, S.; Peris, E. A Rigid Trigonal-Prismatic Hexagold Metallocage That Behaves as a Coronene Trap. *Angew. Chem., Int. Ed.* **2019**, *58*, 6693−6697.
(48) Cai, L. X.; Yan, D. N.; Cheng, P. M.; Xuan, J. J.; Li, S. C.; Zhou, L. P.; Tian, C. B.; Sun, Q. F. Controlled Self-Assembly and Multistimuli-Responsive Interconversions of Three Conjoined Twin-Cages. *J. Am. Chem. Soc.* **2021**, *143*, 2016−2024.
(49) Purba, P. C.; Maity, M.; Bhattacharyya, S.; Mukherjee, P. S. A Self-Assembled Palladium(II) Barrel for Binding of Fullerenes and Photosensitization Ability of the Fullerene-Encapsulated Barrel. *Angew. Chem., Int. Ed.* **2021**, *60*, 14109−14116.
(50) Oldacre, A. N.; Friedman, A. E.; Cook, T. R. A Self-Assembled Cofacial Cobalt Porphyrin Prism for Oxygen Reduction Catalysis. *J. Am. Chem. Soc.* **2017**, *139*, 1424−1427.
(51) Cai, L. X.; Li, S. C.; Yan, D. N.; Zhou, L. P.; Guo, F.; Sun, Q. F. A Water-Soluble Redox-Active Cage Hosting Polyoxometalates for Selective Desulfurization Catalysis. *J. Am. Chem. Soc.* **2018**, *140*, 4869−4876.
(52) Guo, J.; Fan, Y. Z.; Lu, Y. L.; Zheng, S. P.; Su, C. Y. Visible-Light Photocatalysis of Asymmetric [2+2] Cycloaddition in Cage-Confined Nanospace Merging Chirality with Triplet-State Photosensitization. *Angew. Chem., Int. Ed.* **2020**, *59*, 8661−8669.
(53) Chu, D.; Gong, W.; Jiang, H.; Tang, X.; Cui, Y.; Liu, Y. Boosting Enantioselectivity of Chiral Molecular Catalysts with Supramolecular Metal−Organic Cages. *CCS Chem.* **2021**, *3*, 1692−1700.
(54) Howlader, P.; Mondal, B.; Purba, P. C.; Zangrando, E.; Mukherjee, P. S. Self-Assembled Pd(II) Barrels as Containers for Transient Merocyanine form and Reverse Thermochromism of Spiropyran. *J. Am. Chem. Soc.* **2018**, *140*, 7952−7960.
(55) Hasegawa, S.; Meichsner, S. L.; Holstein, J. J.; Baksi, A.; Kasanmascheff, M.; Clever, G. H. Long-Lived C_{60} Radical Anion Stabilized Inside an Electron-Deficient Coordination Cage. *J. Am. Chem. Soc.* **2021**, *143*, 9718−9723.
(56) Durot, S.; Taesch, J.; Heitz, V. Multiporphyrinic Cages: Architectures and Functions. *Chem. Rev.* **2014**, *114*, 8542−8578.
(57) Percástegui, E. G.; Jancik, V. Coordination-Driven Assemblies Based on Meso-Substituted Porphyrins: Metal-Organic Cages and a New Type of Meso-Metallaporphyrin Macrocycles. *Coord. Chem. Rev.* **2020**, *407*, No. 213165.
(58) Lee, S. J.; Hupp, J. T. Porphyrin-Containing Molecular Squares: Design and Applications. *Coord. Chem. Rev.* **2006**, *250*, 1710−1723.
(59) Bar, A. K.; Chakrabarty, R.; Mostafa, G.; Mukherjee, P. S. Self-Assembly of a Nanoscopic $Pt_{12}Fe_{12}$ Heterometallic Open Molecular Box Containing Six Porphyrin Walls. *Angew. Chem., Int. Ed.* **2008**, *47*, 8455−8459.
(60) Lee, H.; Hong, K. I.; Jang, W. D. Design and Applications of Molecular Probes Containing Porphyrin Derivatives. *Coord. Chem. Rev.* **2018**, *354*, 46−73.
(61) Fuertes-Espinosa, C.; Garcia-Simon, C.; Pujals, M.; Garcia-Borras, M.; Gomez, L.; Parella, T.; Juanhuix, J.; Imaz, I.; Maspoch, D.; Costas, M.; Ribas, X. Supramolecular Fullerene Sponges as Catalytic Masks for Regioselective Functionalization of C_{60}. *Chem* **2020**, *6*, 169−186.
(62) Ubasart, E.; Borodin, O.; Fuertes-Espinosa, C.; Xu, Y.; Garcia-Simon, C.; Gomez, L.; Juanhuix, J.; Gandara, F.; Imaz, I.; Maspoch, D.; von Delius, M.; Ribas, X. A Three-Shell Supramolecular Complex Enables the Symmetry-Mismatched Chemo- and Regioselective Bis-Functionalization of C_{60}. *Nat. Chem.* **2021**, *13*, 420−427.
(63) Shi, Y.; Sanchez-Molina, I.; Cao, C.; Cook, T. R.; Stang, P. J. Synthesis and Photophysical Studies of Self-Assembled Multicomponent Supramolecular Coordination Prisms Bearing Porphyrin Faces. *Proc. Natl. Acad. Sci. U.S.A.* **2014**, *111*, 9390−9395.
(64) Yu, G.; Yu, S.; Saha, M. L.; Zhou, J.; Cook, T. R.; Yung, B. C.; Chen, J.; Mao, Z.; Zhang, F.; Zhou, Z.; Liu, Y.; Shao, L.; Wang, S.;

https://doi.org/10.1021/jacsau.2c00245
JACS Au 2022, 2, 1479−1487

Gao, C.; Huang, F.; Stang, P. J.; Chen, X. A Discrete Organoplatinum-(II) Metallacage as a Multimodality Theranostic Platform for Cancer Photochemotherapy. *Nat. Commun.* **2018**, *9*, No. 4335.
(65) Sun, Y.; Chen, C.; Liu, J.; Liu, L.; Tuo, W.; Zhu, H.; Lu, S.; Li, X.; Stang, P. J. Self-Assembly of Porphyrin-Based Metallacages into Octahedra. *J. Am. Chem. Soc.* **2020**, *142*, 17903−17907.
(66) Benavides, P. A.; Gordillo, M. A.; Yadav, A.; Joaqui-Joaqui, M. A.; Saha, S. Pt(ii)-Coordinated Tricomponent Self-Assemblies of Tetrapyridyl Porphyrin and Dicarboxylate Ligands: are They 3D Prisms or 2D Bow-ties? *Chem. Sci.* **2022**, *13*, 4070−4081.
(67) Fujii, S.; Tada, T.; Komoto, Y.; Osuga, T.; Murase, T.; Fujita, M.; Kiguchi, M. Rectifying Electron-Transport Properties through Stacks of Aromatic Molecules Inserted into a Self-Assembled Cage. *J. Am. Chem. Soc.* **2015**, *137*, 5939−5947.
(68) Spenst, P.; Würthner, F. A Perylene Bisimide Cyclophane as a "Turn-On" and "Turn-Off" Fluorescence Probe. *Angew. Chem., Int. Ed.* **2015**, *54*, 10165−10168.
(69) Zhang, D.; Ronson, T. K.; Lavendomme, R.; Nitschke, J. R. Selective Separation of Polyaromatic Hydrocarbons by Phase Transfer of Coordination Cages. *J. Am. Chem. Soc.* **2019**, *141*, 18949−18953.
(70) Zhang, C.; Wang, H.; Zhong, J.; Lei, Y.; Du, R.; Zhang, Y.; Shen, L.; Jiao, T.; Zhu, Y.; Zhu, H.; Li, H.; Li, H. A Mutually Stabilized Host-Guest Pair. *Sci. Adv.* **2019**, *5*, No. eaax6707.
(71) Liu, W.; Bobbala, S.; Stern, C. L.; Hornick, J. E.; Liu, Y.; Enciso, A. E.; Scott, E. A.; Stoddart, J. F. XCage: A Tricyclic Octacationic Receptor for Perylene Diimide with Picomolar Affinity in Water. *J. Am. Chem. Soc.* **2020**, *142*, 3165−3173.
(72) Deposition Numbers 2102359 (for **4**), 2102363 (for **4**⊃**G**$_1$), 2109173 (for **4**⊃**G**$_2$), 2109174 (for **4**⊃**G**$_3$), 2109177 (for **4**⊃**G**$_4$), 2109175 (for **4**⊃**G**$_5$), 2109178 (for **4**⊃**G**$_6$), and 2161223 (for **4**⊃**G**$_{11}$) contain the supplementary crystallographic data for this paper. These data are provided free of charge by the joint Cambridge Crystallographic Data Centre and Fachinformationszentrum Karlsruhe Access Structures Service. www.ccdc.cam.ac.uk/.
(73) Hiroto, S.; Miyake, Y.; Shinokubo, H. Synthesis and Functionalization of Porphyrins through Organometallic Methodologies. *Chem. Rev.* **2017**, *117*, 2910−3043.
(74) Ghogare, A. A.; Greer, A. Using Singlet Oxygen to Synthesize Natural Products and Drugs. *Chem. Rev.* **2016**, *116*, 9994−10034.
(75) Cullen, W.; Turega, S.; Hunter, C. A.; Ward, M. D. Virtual Screening for High Affinity Guests for Synthetic Supramolecular Receptors. *Chem. Sci.* **2015**, *6*, 2790−2794.
(76) Fudickar, W.; Linker, T. Why Triple Bonds Protect Acenes from Oxidation and Decomposition. *J. Am. Chem. Soc.* **2012**, *134*, 15071−15082.
(77) Klaper, M.; Linker, T. Intramolecular Transfer of Singlet Oxygen. *J. Am. Chem. Soc.* **2015**, *137*, 13744−13747.

https://doi.org/10.1021/jacsau.2c00245
JACS Au 2022, 2, 1479−1487